Dynamics of OH Formation in the Photodissociation of *o*-Nitrobenzoic Acid at 295 and 355 nm

Can-Hua Zhou, Shi-Bo Cheng, Ju-Long Sun, Hong-Ming Yin,* Ke-Li Han, and Guo-Zhong He

State Key Laboratory of Molecular Reaction Dynamics, Dalian Institute of Chemical Physics, Chinese Academy of Sciences, Dalian 116023, China

Received: January 19, 2009; Revised Manuscript Received: March 12, 2009

Photodissociation dynamics of *o*-nitrobenzoic acid at 295 and 355 nm is studied by probing the nascent OH photoproduct employing the single-photon laser-induced fluorescence technique. At both of the photolysis wavelengths, the OH fragments are found to be vibrationally cold but have different rotational state distributions. Upon photolysis at 295 nm, the relative population of OH in different rotational states does not follow the Boltzmann equilibrium distribution, whereas upon photolysis at 355 nm, a Boltzmann distribution is observed with a rotational temperature of 1010 ± 100 K. Between the two spin−orbit states, $^2\Pi_{3/2}$ and $^2\Pi_{1/2}$, the former is found to be preferentially populated, and the distribution of the $\Pi(A')$ state for the Λ-doublet is dominant at both of the wavelengths studied. Several possible dissociation pathways of *o*-nitrobenzoic acid leading to formation of the OH fragment are investigated computationally. On the basis of the theoretical and experimental studies, a possible mechanism of OH formation from the photodissociation of *o*-nitrobenzoic acid at 295 and 355 nm is proposed.

1. Introduction

In benzoic acid, the simplest aromatic carboxylic acid, the conjugation interaction between the phenyl ring and the carboxylic group, leads to interesting photophysics and photochemistry. While photodissociation dynamics of aliphatic carboxylic acids has been studied extensively,[1–5] much less is known about aromatic carboxylic acids, especially benzoic acid. Most of the works related to benzoic acid are mainly focused on the complex proton-transfer dynamics of its dimer, and only a few theoretical and experimental studies are devoted to its molecular photophysics and photochemistry. Baba and coworkers[6] found that benzoic acid shows phosphorescence alone with a high quantum yield. It was inferred that intersystem crossing to the lowest triplet state occurs very efficiently in benzoic acid. Kamei et al.[7] employed the sensitized phosphorescence excitation spectroscopy to observe the electronic excited states of benzoic acid in supersonic jets. The two sharp bands at 35923 and 35943 cm^{-1} were assigned to the origins of the two rotational isomers of benzoic acid. Meijer et al.[8] used the technique of laser desorption followed by jet cooling to identify the $S_0 \rightarrow S_1$ absorption spectrum of benzoic acid in the gas phase. The $S_0 \rightarrow S_1$ band origin was determined to be located at 35960 cm^{-1}, and the rate of the intersystem crossing to the triplet state was very fast. Frequencies and intensities of the IR-active modes for benzoic acid were determined from ion dip spectroscopy and density functional calculation.[9] In addition, a few experimental and theoretical investigations[10–12] have been performed to probe the decarboxylation mechanisms of benzoic acid and to characterize the spectroscopic properties of its derivatives with water. Very recently, we investigated the photodissociation of benzoic acid at different photolysis wavelengths of 266 and 280−294 nm[13,14] and found OH to be formed after the direct cleavage of the C−OH bond. However, no OH fluorescence signal was observed upon photolysis of benzoic acid at 295 nm.[14] In continuation of our earlier work, we studied photodissociation of *o*-nitrobenzoic acid, *o*-$C_6H_4(NO_2)COOH$, at 295 and 355 nm to understand the effect of the chromophore NO_2 on its excitation and dynamics of dissociation. The nitro substitution may change the dissociation mechanism of aromatic carboxylic acids due to its strong electron-withdrawing effect. The present study might provide new insights into the photophysics and photochemistry of nitroaromatic compounds, that is, possible H-atom transfer. Some other nitroaromatic compounds have been investigated recently. The OH fragment, as one of the photodissociation products after the UV excitation, has been directly observed in the photodissociation of *o*-nitrotoluene,[15–17] *o*-nitrophenol,[18] and *o*-nitrobenzaldehyde[19] using the multimass ion imaging technique or the fluorescence spectroscopy technique. In addition, it is worthwhile to investigate, both experimentally and theoretically, the possible dissociation channels of OH as no photochemical dissociation study on *o*-nitrobenzoic acid in the gas phase has been reported so far in the literature, to the best of our knowledge.

In the present study, we have detected the nascent OH photoproduct by employing the single-photon laser-induced fluorescence (LIF) technique after photolysis of the excited *o*-nitrobenzoic acid under collision-free conditions. The photolysis was carried out at 295 and 355 nm to investigate the influence of excitation wavelength on the dissociation channel. We have also carried out ab initio theoretical calculations to investigate the probable channels that lead to formation of OH and characterize the nature of the transition states. According to the experimental results and the theoretical calculations, a possible mechanism of *o*-nitrobenzoic acid photodissociation leading to formation of OH is proposed.

2. Experimental Section

The experimental setup used in the present LIF work has been described in detail elsewhere.[20,21] Here, only a brief description about the apparatus is given. The second-harmonic output (532

* To whom correspondence should be addressed. Fax: +86 411 84675584. E-mail address: hm_yin@dicp.ac.cn.

10.1021/jp900567u CCC: $40.75
Published on Web 04/07/2009

nm) of a seeded Nd:YAG laser (Spectra-Physics, PRO-190) was used to pump a dye laser (Coherent, Scanmate-PRO), which generated the wavelength-tunable laser pulses. The dye laser was operated using rhodamine B dye, of which the corresponding fundamental wavelength tuning range is 577−601 nm. The output of the dye laser was checked by a laser wavelength meter (Coherent) and then introduced into a harmonic generator (Coherent, Scanmate-SHG) to produce the frequency-doubled UV laser pulses in the 288.5−300.5 nm region, which were used for the photolysis laser pulses. There was another dye laser (Lumonics, HD-500) pumped by a second-harmonic output of a Nd:YAG laser (Spectra-Physics, GCR-170). This dye laser was operated using DCM dye with a fundamental wavelength tuning range of 600−640 nm. The output of the dye laser was then introduced into a harmonic generator (Lumonics, HT-1000) to produce the frequency-doubled laser pulses in the 300−320 nm region, which were used for the probe laser pulses. Both the photolysis and probe beams were collinearly counter propagated through the center of the photolysis cell. The probe laser was delayed 15 ns with respect to the photolysis laser, which was controlled by a generator (SRS, DG535). This delay period was sufficient to separate the two laser pulses and was short enough to make collision effects negligible under the pressure (typically 200 mTorr) during the experiments. Moreover, the third-harmonic output (355 nm) of the Nd:YAG laser (Spectra-Physics, GCR-170) was also used for the photolysis laser pulse. In our experiments, the pulse energies were about 0.02 and 1.5 mJ for the probe and photolysis laser beams, respectively.

The OH fragment was probed by exciting the $A^2\Sigma^+(v'=0) \leftarrow X^2\Pi(v''=0)$ transition of OH and monitoring the subsequent $A \rightarrow X$ fluorescence. The fluorescence of the OH fragment was collected by a photomultiplier tube (PMT, Hamamatsu CR161). A suitable band filter (λ_{center} = 310 nm, full width at half-maximum (fwhm) = 15 nm) was placed between the collecting lens and the PMT to cut off scattering from the photolysis laser and the probe laser. The signal was gate-integrated by a boxcar (SRS, SR250), A/D converted by a homemade interface, and stored in a personal computer. In the experiments, a saturation effect was avoided by keeping the laser beam energies low enough to observe a linear behavior of the LIF intensity with respect to the variations of the powers of each laser and the sample pressure of the photolysis cell.

o-Nitrobenzoic acid (≥99.5%) was purchased from Shengyang Lianbang Chemicals Reagents Company and used without further purification. During the experiment, the sample was heated to 410 K, the helium carrier gas was bubbled through the sample, and the gas mixture was expanded into the photolysis cell.

3. Computational Details

Ab initio molecular orbital (MO) calculations were performed, using the Gaussian 03 program,[22] to investigate the potential energy surface (PES) for the OH formation channel from the lowest triple state of *o*-nitrobenzoic acid. The geometries of the ground and the lowest triple electronic states of *o*-nitrobenzoic acid, the various possible intermediate products, the radical species, and the transition-state structures were optimized with the B3LYP theory, using the 6-311+G(d,p) basis set. The electronic energies corresponding to the optimized geometries were calculated at the same level, including the zero-point energy (ZPE) correction. The harmonic vibrational frequencies and the force constants were calculated to ensure the stationary points on the potential energy surfaces to be true saddle points.

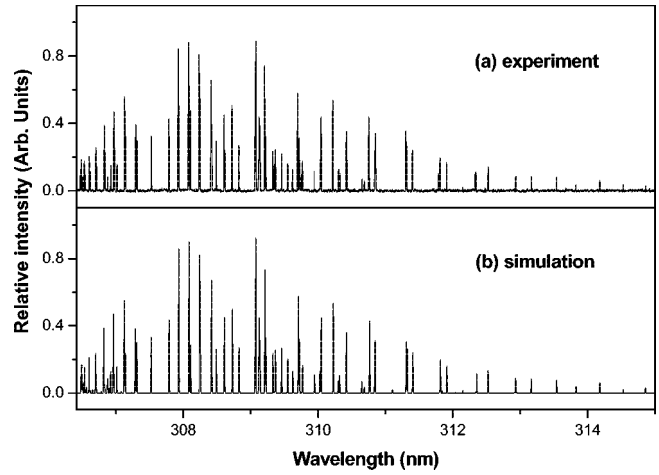

Figure 1. A comparison of the LIF excited spectra of the nascent OH ($A^2\Sigma^+(v'=0) \leftarrow X^2\Pi(v''=0)$) fragment from the photodissociation of *o*-nitrobenzoic acid at 295 nm: (a) experiment and (b) simulation.

All of the transition-state (TS) structures calculated have only one imaginary frequency and one negative eigenvalue of the force constant matrix. Time-dependent density functional theory (TD-DFT) at the B3LYP/6-311+G(d,p) basis set was employed to calculate the vertical excitation energies of the low-lying electronic states based on the ground-state geometry of *o*-nitrobenzoic acid and predicted the nature and oscillator strength of an electronic transition.

4. Experimental Results

The LIF spectra of the OH fragment from *o*-nitrobenzoic acid photolysis at 295 and 355 nm were recorded by scanning the OH $A^2\Sigma^+(v'=0) \leftarrow X^2\Pi(v''=0)$ transition in the 306−315 nm range. The measured OH LIF signal was found to be linearly dependent on the photolysis and probe laser powers, indicating that the photodissociation of *o*-nitrobenzoic acid was a single-photon process and that the fluorescence was not saturated. At both of the photolysis wavelengths, the nascent OH radical was formed in the vibrational ground state. Figure 1a shows the experimental LIF excitation spectrum of the (0,0) band of the nascent OH, formed upon photolysis at 295 nm. In order to precisely assign the J'' levels of the OH populated in the dissociation process, it is necessary to compare the experimental spectrum with the simulated one calculated from the known spectroscopic constants.[23] The rotational state population $N(J'',v'')$ in the ground electronic state could be obtained from the intensities of the observed LIF rotational lines. The relationship between the intensities of the fluorescence signal (I_F) and the rovibrational state populations $N(J'',v'')$ is expressed by

$$I_F \propto \frac{N(J'', v'')q_{v'v''}S_{J'J''}f(\nu, \nu_0)}{(2J'' + 1)} \quad (1)$$

where $q_{v'v''}$ are the known Franck−Condon factors for the OH A−X transition,[24] $S_{J'J''}$ are the line strengths for the OH A−X one-photon rotational transitions,[25] and $f(\nu,\nu_0) = \rho(\nu_0) \exp(-\alpha(\nu - \nu_0)^2)$ is the laser intensity function. The simulated spectrum of the OH (0,0) band corresponding to the photolysis wavelength of 295 nm is plotted in Figure 1b. The excitation LIF spectrum observed upon photolysis at 355 nm is similar to that at 295 nm and hence is not shown.

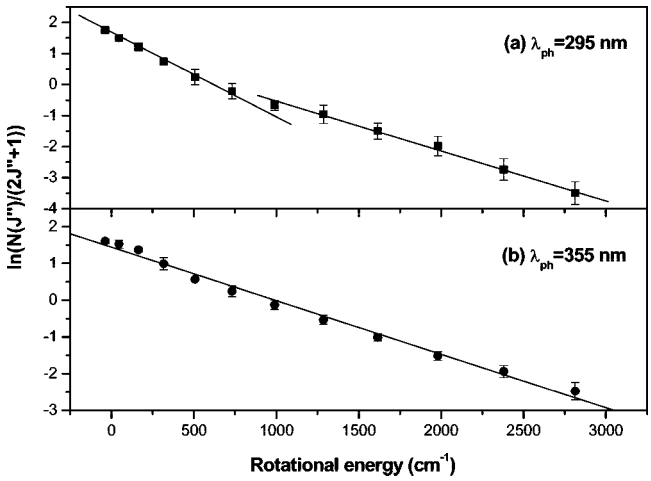

Figure 2. The Boltzmann plot for the rotational state distributions of the nascent OH fragment generated from the photolysis of *o*-nitrobenzoic acid at (a) 295 and (b) 355 nm. The plot appears to be curing at 295 nm, indicating that the population of OH is not at equilibrium over all of the rotational levels, while at 355 nm, the solid line is the best fit to the data points and represents a rotational temperature of 1010 ± 100 K.

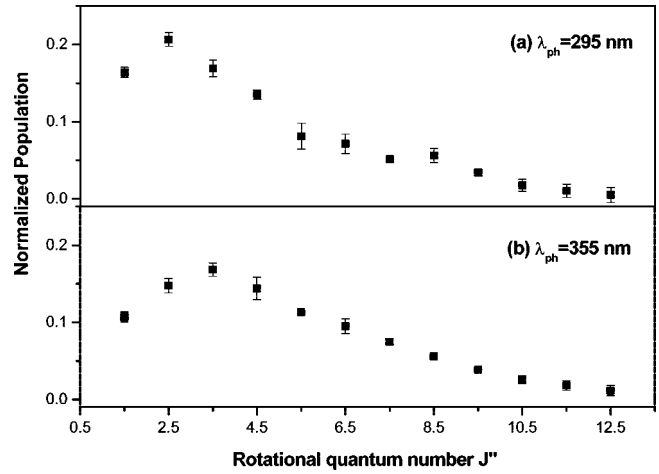

Figure 3. Rotational population distribution of the OH fragments generated from the photodissociation of *o*-nitrobenzoic acid at (a) 295 and (b) 355 nm.

The OH transitions are labeled following Hund's case (a). The P, Q, or R branches are for cases in which $\Delta J = -1$, 0, or 1, and the subscript 1 or 2 represents the different spin−orbit states $^2\Pi_{3/2}$ or $^2\Pi_{1/2}$, respectively. According to the parity selection rule (+ ↔ −), the Q branch only corresponds to the Π(A″) state, while the P and R branches are attributed to the Π(A′) state. Spin−orbit coupling and the Λ-doublet ratios are calculated from the relative population of different rotational states. Detailed analysis of the quantum state distributions of the OH fragment is presented as follows.

4.1. Rotational State Distribution. The OH rotational distributions at 295 and 355 nm photolysis of *o*-nitrobenzoic acid are determined by analyzing of P_1 and P_2 rotational lines because these lines are mostly free from interference from other lines. In order to compare the measurements of each rotational level, the intensities of the observed LIF rotational lines have been normalized with respect to the pressure in the photolysis cell, the energies of the probe laser, and the photolysis laser. On the basis of the normalized experimental data, the rotational state distribution could be characterized by a Boltzmann temperature. The equation of the Boltzmann population distribution is expressed as

$$\ln \frac{N(J'')}{(2J''+1)} = \frac{-\varepsilon(J'')hc}{kT_R} + \text{constant} \qquad (2)$$

The Boltzmann plots of the relative rotational state distributions of the (0,0) band of OH, formed upon photodissociation of *o*-nitrobenzoic acid at 295 and 355 nm, are shown in Figure 2. It is evident that upon photolysis at 295 nm (Figure 2a), the rotational population distribution is more scattered in the lower energy range, and the plot appears to be curving, indicating that the population of the nascent OH(v''=0,J'') fragment is not an equilibrium over all of the rotational levels J''. In contrast, upon photolysis at 355 nm (Figure 2b), the rotational populations are found to follow the Boltzmann distribution, characterized by a rotational temperature of 1010 ± 100 K. The normalized rotational population distributions of OH upon photolysis at 295 and 355 nm are shown in Figure 3. Obviously, there exist some differences between those two rotational distributions, although those are both extended to $J'' = 12.5$. Additionally, the corresponding rotational energies $E_{v''}^{rot}$ of the ground state $X^2\Pi(v''=0)$ are calculated to be 1.6 ± 0.1 and 1.9 ± 0.2 kcal/mol at 295 and 355 nm, respectively, using $E_{v''}^{rot} = \sum_{J''} P(J'')\varepsilon(J'')$, where $P(J'')$ is the relative state population and $\varepsilon(J'')$ is the energy of a given rotational state. The internal energy of OH upon photolysis of *o*-nitrobenzoic acid at 295 nm is similar to that at 355 nm, although the photon energy at 295 nm is about 16 kcal/mol higher than that at 355 nm. Such behavior of energy partitioning is also observed in the photodissociation of *o*-nitrotoluene[17] at 193 and 248 nm.

In addition, to see whether any OH is produced in the $v'' = 1$ level, the OH $A^2\Sigma^+(v'=1) \leftarrow X^2\Pi(v''=1)$ transition was scanned at both 295 and 355 nm. However, no LIF signal of the OH photofragment ($X^2\Pi$, $v'' = 1$) was observed from the photodissociation of *o*-nitrobenzoic acid at each photolysis wavelength, which suggests that the OH fragments are both mostly populated in $v'' = 0$ in our experiments.

4.2. Spin−Orbit State Distribution. Since the electronic spin has a value of 1/2 in the OH radical, the interaction of the electronic spin with the orbital angular momentum splits the $X^2\Pi$ state into two spin orbit components, $^2\Pi_{3/2}$ and $^2\Pi_{1/2}$. Populations of the two spin−orbit states, $^2\Pi_{3/2}$ and $^2\Pi_{1/2}$, can be obtained from the intensities of $P_1(Q_1)$ and $P_2(Q_2)$ lines, respectively. The ratios of the population of the $^2\Pi_{3/2}$ and $^2\Pi_{1/2}$ states are plotted versus the rotational quantum number J'' in Figure 4 upon photolysis at 295 and 355 nm. As can be seen from the plot, the OH fragment exhibits a preferential population of the $^2\Pi_{3/2}$ state with the relative values of 1.6 ± 0.2 and 1.5 ± 0.2 upon photolysis at 295 and 355 nm, respectively. The distinct deviation of the measured spin−orbit ratio from the statistical value could be explained partly based on the energy difference between these two states; the $^2\Pi_{1/2}$ state lies higher in energy than the $^2\Pi_{3/2}$ state at the same J''. The preferential population of the $^2\Pi_{3/2}$ state also indicates a coupling between the initially prepared excited singlet state and a nearby triplet state or the result of inelastic scattering between the recoiling fragments.[26,27]

4.3. Λ-Doublet State Distribution. The Λ-doublet splitting arises due to the interaction between the orbital angular momentum and nuclear rotation, and this interaction is of different magnitude for two Λ-doublet states, Π(A′) and Π(A″). These two states in the OH radical are created by different orientations of the Π lobes with respect to the plane of rotation.

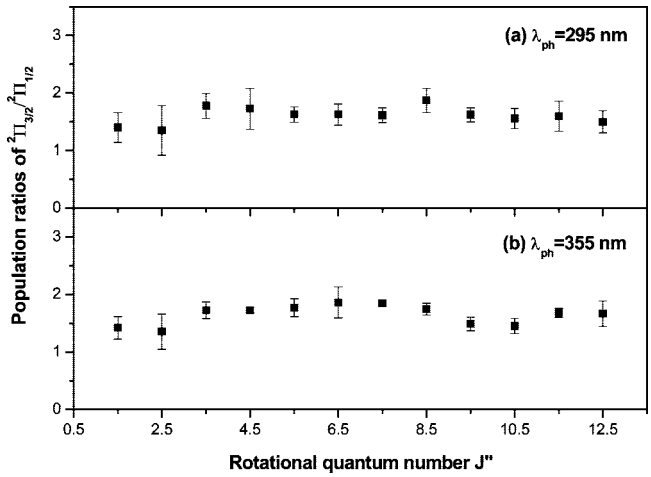

Figure 4. Ratios of the population of $^2\Pi_{3/2}/^2\Pi_{1/2}$ versus the rotational quantum number J'' of the nascent OH($X^2\Pi$,v''=0) fragment after *o*-nitrobenzoic acid photolysis at (a) 295 and (b) 355 nm. The $^2\Pi_{3/2}$ state is preferentially populated at both of the photolysis wavelengths.

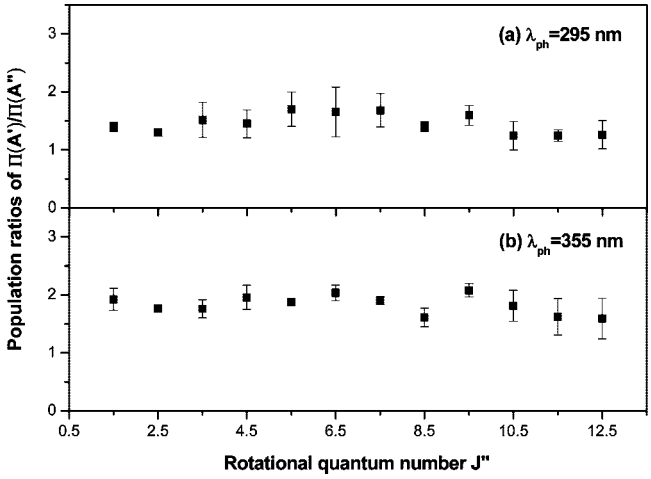

Figure 5. The relative Λ-doublet population versus the rotational quantum number J'' of the nascent OH($X^2\Pi$,v''=0) fragment from the photolysis of *o*-nitrobenzoic acid at (a) 295 and (b) 355 nm. The Π(A′) state is populated in preference to the Π(A″) state at both of the photolysis wavelengths.

In the Π(A′) state, the pπ lobe lies in the plane of rotation, whereas in the Π(A″) state, the pπ lobe is perpendicular to the plane of rotation. As mentioned earlier, the Q branch is used for detecting the OH fragment in the Π(A″) state, whereas the R and P branches are used for that in the Π(A′) state. Thus, the R/Q (or P/Q) intensity ratios represent the ratios of the Λ-doublet, which give information about the relative population of the OH fragment in the Π(A′) and Π(A″) states.[28] In Figure 5, the Λ-doublet population ratios for the $^2\Pi_{3/2}$ state obtained from the P_1/Q_1 ratio are shown with the function of the rotational quantum number J'' upon photolysis at 295 and 355 nm. It can be seen from the figure that the states are unequally populated, with the Λ-doublet population ratios (Π(A′)/Π(A″)) of 1.5 ± 0.2 and 1.7 ± 0.2 upon photolysis at 295 and 355 nm, respectively, implying a preferential population of OH in the Π(A′) state at both of the photolysis wavelengths. This result suggests that the pπ electronic orbital of the OH radical is predominantly in its plane of rotation.

5. Discussion

Ab initio molecular orbital (MO) calculations were performed to investigate the mechanism of OH formation from *o*-nitrobenzoic acid upon photolysis at 295 and 355 nm. The optimized structures of the lowest triplet electronic state of *o*-nitrobenzoic acid, the intermediate products, the radical species, and the transition states are depicted in Figure 6, where the atom labeling scheme is also given. Detailed structural parameters of species involved, together with the structure of the ground state, are available in the Supporting Information. One minimum-energy structure on the lowest triplet surface of *o*-nitrobenzoic acid, T_1 (Mol1), has a nonplanar geometry, which is similar to the S_0 structure. There are minor changes only in the nitro group from S_0 to T_1, with the two N−O bond lengths elongated from 1.222 to 1.312 Å, indicating the loss of the N═O double bond character. With respect to the S_0 state zero level, the T_1 state has a relative energy of 53.3 kcal/mol at the B3LYP/6-311+G(d,p) level.

Calculations on the three lowest excited states of *o*-nitrobenzoic acid (S_1, S_2, and T_1) were also carried out by employing the time-dependent density functional theory (TD-DFT) at the B3LYP/6-311+G(d,p) level based on the S_0 geometry. The S_1 state, with the vertical excitation energy of 3.78 eV, involves transition mainly from the highest occupied molecular orbital (HOMO) to the lowest unoccupied molecular orbital (LUMO), which is the $\pi_{whole}-\pi^*_{whole}$ transition. Here, the π_{whole} means the big π orbital including the phenyl group and the C11 and N16 atoms. The S_2 state, with the vertical excitation energy of 4.27 eV, is generated by mixed transitions mainly from the second highest occupied molecular orbital (HOMO-1) to the LUMO, which is the $\pi_{phenyl+C}-\pi^*_{whole}$ transition. The T_1 state involves mainly the $\pi-\pi^*$ transition in the nitro group with the vertical excitation energy of 2.89 eV. In addition, the internal energy of *o*-nitrobenzoic acid (at 410 K) was determined to be about 9.6 kcal/mol at the B3LYP/6-311+G (d,p) level of theory.

As reported earlier,[29] the rate of the internal conversion in the excited singlet states of *o*-nitrobenzoic acid in ethanol is very fast, and the lifetime of the S_1 state is found to be very short. The T_1 formation is very efficient via intersystem crossing, and its quantum yield is found to be greater than 0.70. Additionally, as mentioned above, the preferential population of the $^2\Pi_{3/2}$ state is observed, indicating a coupling between the initially prepared excited singlet state and a nearby triplet state.[26] Moreover, upon photolysis at 295 and 355 nm, the similar low internal energy of the OH fragment may be due to the presence of a considerable exit barrier in the reaction channel, which implies that OH is formed on an electronically excited potential energy surface since dissociation from the ground electronic state is essentially barrierless.[2–5] Thus, it can be assumed that the competing dissociation and rearrangement channels of *o*-nitrobenzoic acid occur on the lowest triplet T_1 electronic state.

Thus, considering the internal energy of the parent molecule and the photon energy used in the present work, the initial excitation at 295 and 355 nm leads to population of *o*-nitrobenzoic acid in the S_2 and S_1 states, respectively, which is consistent with its UV absorption spectrum.[30] Then, from those states, it relaxes to the lower T_1 state mainly by internal conversion and intersystem crossing processes. Finally, it dissociates from the T_1 state to generate OH, as suggested by our calculations of the transition-state structures for the OH channels from this electronic state.

According to the above discussion, the T_1 state is likely the dominant electronic state to produce OH from *o*-nitrobenzoic acid photodissociation. Therefore, we have carried out ab initio calculations on different channels from the T_1 electronic state of *o*-nitrobenzoic acid. The relative energy diagram is depicted

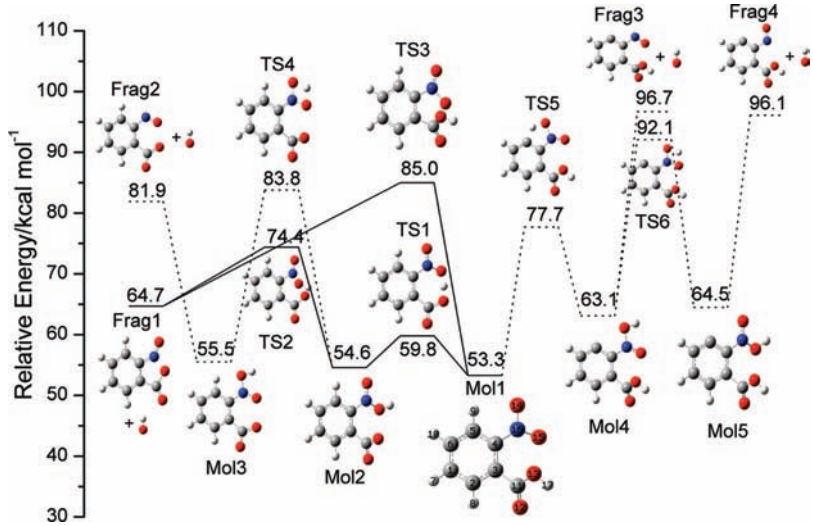

Figure 6. Schematic energy diagram of possible channels of OH formation from photodissociation of *o*-nitrobenzoic acid in the T_1 state and the optimized geometries of the isomers, transition states (TS), and dissociation products calculated at the B3LYP/6-311+G(d,p) level, where all energies are given in kcal/mol and the atom labeling is given in the T_1 structure. The two reasonable pathways of OH formation are shown as solid lines.

schematically in Figure 6. Four possible pathways of OH formation from *o*-nitrobenzoic acid are described in the following.

The first pathway involves the H17 migration and isomerization from Mol1 to Mol2 and further dissociation to free two products, OH and Frag1. In the first step of this pathway, H17 undergoes a shift to O15. This leads to the formation of Mol2. This step involves a transition state TS1, with a small barrier of 6.5 kcal/mol above Mol1 in energy. In the subsequent step, the N−OH bond breaks, forming OH and Frag1. For this step, a transition state TS2 with an exit barrier of 19.8 kcal/mol could be located. The combined energy of these two products lies at 64.7 kcal/mol above that of the S_0 minimum. Additionally, the TS2 state is 10.6 kcal/mol lower than the TS3 state (vide infra) in energy. Thus, this pathway of the H17 migration is likely to play an important role in the dissociation of *o*-nitrobenzoic acid to generate OH.

The second possible pathway is the dissociation through direct breaking of the C−OH bond in the carboxylic group, producing also the two radicals, OH and Frag1. In this pathway of OH formation, the step is a concerted process involving the simple C−OH bond cleavage with the simultaneous intramolecular rearrangement. This concerted step involves a transition state TS3 with an activation barrier of 31.7 kcal/mol above Mol1. It is worthwhile to note that Frag1 has a planar geometry, with all of the atoms lying in the same plane. Therefore, there exists a strong p−π conjugation interaction in Frag1, whereas the interaction between the carbonyl group and the aromatic ring is weaker in the fragment C_6H_5CO upon photolysis of benzoic acid. This might be the reason why the OH signal could be detected from photolysis of *o*-nitrobenzoic acid but not from photolysis of benzoic acid at the same photolysis wavelength of 295 nm.[14] Hence, this concerted pathway seems to be a reasonable channel for the dissociation of *o*-nitrobenzoic acid to generate OH.

The third possible pathway is the further isomerization from Mol2 to Mol3 and then the cleavage of the N−OH bond. This isomer Mol3 can produce OH via the N−OH bond cleavage, without an apparent transition state. In the isomerization step, there exists a transition state TS4 with a high barrier of 29.2 kcal/mol above Mol2. Moreover, Frag2 is 17.2 kcal/mol higher than Frag1 in energy. Therefore, due to the high combined energy and the high barrier necessary to overcome, this channel does not have any advantage compared with the first pathway for OH formation.

The forth possible pathway involves the H9 migration and isomerization to Mol4 and further dissociation to generate OH and Frag3. Mol4 also can rearrange to another isomer Mol5 via a transition state TS6. These two isomers can both undergo the N−OH bond cleavage to produce OH. The combined energies of those products, via dissociation of Mol4 and Mol5, are 96.7 and 96.1 kcal/mol, respectively. These combined energies are much higher compared with those in the other three pathways. Therefore, the contribution of this pathway, starting with the N−OH bond scission in Mol4 and Mol5, which involves the H9 migration, can be negligible.

According to the above discussion, it is likely that the OH radical can be produced mostly through the H17 migration pathway and the concerted pathway. From the potential energy scheme (solid line) given in Figure 6, it can be seen that in the case of the 355 nm excitation (80.5 kcal/mol), the concerted pathway is not feasible in energy if we do not consider the internal energy of the parent molecule (9.6 kcal/mol); therefore, this probability of OH formation could be small compared with that in the H17 migration pathway, while the dissociation of *o*-nitrobenzoic acid is energetically feasible through the two pathways with a photon of 295 nm (96.9 kcal/mol). Thus, on the basis of the available photon energy, it is not possible to distinguish these two pathways of OH formation at 295 nm. Namely, upon 355 nm excitation, OH mainly comes from the H17 migration pathway, whereas in the case of 295 nm, OH can come from either the concerted pathway or the H17 migration pathway, or maybe from both.

In the present experiments on the photodissociation of *o*-nitrobenzoic acid at 295 and 355 nm, the rotational population pattern in the OH product has been found to be distinctly different, as shown in Figures 2 and 3. Upon photolysis at 295 nm, the nascent OH fragment does not have an equilibrium distribution in all of the rotational levels, as indicated by the curving of the Boltzmann plots. Very similar results were obtained by Sengupta et al. during photodissociation of 2-nitropropane and 2-methyl-2-nitropropane at both 248 and 193 nm.[31] In the case of OH generation by one-photon UV photolysis

of 2-nitropropane at 193 nm under collisionless conditions, the populations of the lower rotational states (within 800 cm^{-1} rotational energy) show a linear Boltzmann distribution, with a temperature of about 600 K. If we analyze carefully (Figure 2a), the initial points of lower energies up to 1000 cm^{-1}, in the present study also, lie on a straight line, with a lower rotational temperature of 570 K, and the later points at higher energies show a higher rotational temperature of 980 K. It is of interest to note that the lower rotational temperature (570 K) observed in the present study is not very different from that (595 K) observed for the rotational state distribution of OH in the previous study of benzoic acid,[14] which suggests that those OH products may be generated through the same and direct channel, and the higher rotational temperature (980 K) is closer to that (1070 K) observed for the rotational distribution of OH in the dissociation of 2-nitrophenol,[18] which suggests that those OH products may both be generated through the H migration channel. The curving of the Boltzmann plot can be due to either formation of two types of OH fragments from two different mechanisms, each with a rotational equilibrium corresponding to a rotational temperature, or formation of OH fragments by a single mechanism with a nonequilibrium distribution in the rotational states. In contrast, the population of the OH fragment at 355 nm is found to follow the Boltzmann distribution, characterized by a rotational temperature of 1010 ± 100 K. Interestingly, this rotational temperature is close to those (980 and 1080 K) observed for the higher rotational energy states of OH at 295 nm and for the rotational distribution of OH in the dissociation of 2-nitrophenol,[18] indicating that those OH radicals might be formed from the common pathway. Thus, it appears that the mechanism of OH formation from the photolysis of *o*-nitrobenzoic acid at 295 nm is different from that at 355 nm.

In addition, *o*-nitrobenzoic acid dissociates to produce OH and Frag1 dominantly either through the first pathway or through the second pathway at both photolysis wavelengths, taking the internal energy of the parent molecule at 410 K into account; therefore, the theoretical available energy for partitioning into product states is 41.8 and 25.4 kcal/mol at 295 and 355 nm, respectively. However, in the present investigation, only 1.6 and 1.9 kcal/mol of the available energy is distributed into OH internal energy upon photolysis at 295 and 355 nm, respectively. The low internal energy distribution of OH from *o*-nitrobenzoic acid photolysis is very similar to that of some carboxylic acids,[2–5,17] which may indicate the presence of a considerable barrier in the exit channels. This is quite consistent with our above calculation results on the T_1 state of *o*-nitrobenzoic acid.

Furthermore, the relative population of the Λ-doublet of OH provides the exit channel dynamics in the bond cleavage process. As the ratio, $\Pi(A')/\Pi(A'')$ is similar at both of the wavelengths studied, the exit channel dynamics of OH formation seems to be similar. The nonstatistical ratio of the Λ-doublet suggests that the transition states for the OH formation channels are slightly nonplanar in nature. The optimized structures of the TS2 and TS3 states by DFT calculations are nonplanar, which further support the proposed dissociation mechanism. Since the structures of the TS2 and TS3 states are similar, it is not surprising that the Λ-doublet ratio for both of the photolysis wavelengths is similar.

Hence, we conclude that upon photolysis of *o*-nitrobenzoic acid at 355 nm, the nascent OH fragment is formed mainly via the transition state TS2, involving the H17 atom migration from the carboxylic group to the nitro group, whereas in the case of 295 nm, it is formed mainly via both the transition state TS3, involving the direct C−OH bond scission in the carboxylic group, and the transition state TS2, involving the H17 atom migration. We cannot clarify which one is dominant for OH formation at 295 nm at present. The measurement of the OH formation time would provide good evidence to distinguish those two pathways, and the measurement of the OH translational energy distribution by Doppler analyses would also be very helpful to clarify the reaction mechanism further. A higher level of theoretical study, having better quantitative accuracy, may be useful to understand this system more holistically.

6. Conclusions

The formation of the OH fragment was detected from the photodissociation of *o*-nitrobenzoic acid at 295 and 355 nm using the state-selective LIF technique. At both of the photolysis wavelengths, the nascent OH fragment was found to be vibrationally cold. A nonequilibrium distribution of the rotational population was observed at 295 nm, indicated by curving of the Boltzmann plots, whereas a perfect Boltzmann distribution was shown with a rotational temperature of 1010 ± 100 K at 355 nm, which indicates that the mechanism of OH formation at 295 nm is different from that at 355 nm. At both of the wavelengths studied, the $^2\Pi_{3/2}$ state of OH is populated preferentially implying participation of a nearby triplet state, and the dominant population of the $\Pi(A')$ Λ-doublet state suggests a nonplanar transition-state geometry for the OH channels. Ab initio calculations were carried out to better understand and compare the various possible pathways of OH formation. These barriers in each possible pathway were observed in our calculations, and the corresponding transition states were also characterized on the T_1 state. Finally, on the basis of the experimental results and the theoretical calculations, it is concluded that upon photolysis at 295 nm, OH is formed via both the concerted pathway, involving the direct C−OH bond scission in the carboxylic group and the simultaneous intramolecular rearrangement, and the H migration pathway, involving the H17 atom migration from the carboxylic group to the nitro group, whereas in the case of 355 nm photolysis, it is formed after the N−OH bond cleavage in the rearranged structure Mol2, $C_6H_4NO(OH)CO_2$, involving the H17 atom migration.

Acknowledgment. The authors wish to thank the reviewers for helpful discussion. This work was financially supported by NSFC (20721004, 20833008) and the knowledge innovation program of the Chinese Academy of Sciences (DICP R200603). One of the authors (Hong-Ming Yin) wishes to express thanks to SRF for ROCS, SEM.

Supporting Information Available: Structures of all stationary points reported in the present work. This material is available free of charge via the Internet at http://pubs.acs.org.

References and Notes

(1) Kong, H. T.; Shin, S. K.; Kim, S. K.; Kim, H. L.; Park, C. R. *J. Phys. Chem. A* **2001**, *105*, 6775.
(2) Kumar, A.; Upadhyaya, H. P.; Naik, P. D.; Maity, D. K.; Mittal, J. P. *J. Phys. Chem. A* **2002**, *106*, 11847.
(3) Upadhyaya, H. P.; Kumar, A.; Naik, P. D.; Sapre, A. V.; Mittal, J. P. *J. Chem. Phys.* **2002**, *117*, 10097.
(4) Kumar, A.; Upadhyaya, H. P.; Naik, P. D. *J. Phys. Chem. A* **2004**, *108*, 6275.
(5) Pushpa, K. K.; Upadhyaya, H. P.; Kumar, A.; Naik, P. D.; Bajaj, P. N. *J. Chem. Phys.* **2004**, *120*, 6964.
(6) Baba, H.; Kitamura, M. *J. Mol. Spectrosc.* **1972**, *41*, 302.
(7) Kamei, S. I.; Abe, H.; Mikami, N.; Ito, M. *J. Phys. Chem.* **1985**, *89*, 3636.

(8) Meijer, G.; Vries, M. S.; Hunziker, H. E.; Wendt, H. E. *J. Phys. Chem.* **1990**, *94*, 4394.
(9) Bakker, J. M.; MacAleese, L.; Helden, G. V.; Meijer, G. *J. Chem. Phys.* **2003**, *119*, 11180, and references therein.
(10) Li, J.; Brill, T. B. *J. Phys. Chem. A* **2003**, *107*, 266.
(11) Ruelle, P. *J. Mol. Struct.: THEOCHEM* **1987**, *8*, 158.
(12) He, Y. G.; Wu, C. Y.; Kong, W. *J. Phys. Chem. A* **2005**, *109*, 2809.
(13) Wei, Q.; Sun, J. L.; Yue, X. F.; Yin, H. M.; Han, K. L. *Chem. Phys. Lett.* **2007**, *448*, 11.
(14) Wei, Q.; Sun, J. L.; Yue, X. F.; Cheng, S. B.; Zhou, C. H.; Yin, H. M.; Han, K. L. *J. Phys. Chem. A* **2008**, *112*, 4727.
(15) Chen, S. C.; Xu, S. C.; Diau, E.; Lin, M. C. *J. Phys. Chem. A* **2006**, *110*, 10130.
(16) Lin, M. F.; Lee, Y. T.; Ni, C. K.; Lin, M. C. *J. Chem. Phys.* **2007**, *126*, 064310−1.
(17) Sengupta, S.; Upadhyaya, H. P.; Kumar, A.; Dhanya, S.; Naik, P. D.; Bajaj, P. N. *Chem. Phys. Lett.* **2008**, *452*, 239.
(18) Wei, Q.; Yin, H. M.; Sun, J. L.; Yue, X. F.; Han, K. L. *Chem. Phys. Lett.* **2008**, *463*, 340.
(19) Cheng, S. B.; Zhou, C. H.; Yin, H. M.; Sun, J. L.; Han, K. L. *ChemPhysChem* **2009**, *10*. DOI: 10.1002/cphc.2008.0735.
(20) Yin, H. M.; Sun, J. L.; Li, Y. M.; Han, K. L.; He, G. Z. *J. Chem. Phys.* **2003**, *118*, 8248.
(21) Zhou, C. H.; Cheng, S. B.; Sun, J. L.; Yin, H. M.; Han, K. L.; He, G. Z. *Chem. Phys. Lett.* **2008**, *466*, 27.
(22) Frisch, M. J.; Trucks, G. W.; Schlegel, H. B.; Scuseria, G. E.; Robb, M. A.; Cheeseman, J. R.; Montgomery, J. A., Jr.; Vreven, T.; Kudin, K. N.; Burant, J. C.; Millam, J. M.; Iyengar, S. S.; Tomasi, J.; Barone, V.; Mennucci, B.; Cossi, M.; Scalmani, G.; Rega, N.; Petersson, G. A.; Nakatsuji, H.; Hada, M.; Ehara, M.; Toyota, K.; Fukuda, R.; Hasegawa, J.; Ishida, M.; Nakajima, T.; Honda, Y.; Kitao, O.; Nakai, H.; Klene, M.; Li, X.; Knox, J. E.; Hratchian, H. P.; Cross, J. B.; Bakken, V.; Adamo, C.; Jaramillo, J.; Gomperts, R.; Stratmann, R. E.; Yazyev, O.; Austin, A. J.; Cammi, R.; Pomelli, C.; Ochterski, J. W.; Ayala, P. Y.; Morokuma, K.; Voth, G. A.; Salvador, P.; Dannenberg, J. J.; Zakrzewski, V. G.; Dapprich, S.; Daniels, A. D.; Strain, M. C.; Farkas, O.; Malick, D. K.; Rabuck, A. D.; Raghavachari, K.; Foresman, J. B.; Ortiz, J. V.; Cui, Q.; Baboul, A. G.; Clifford, S.; Cioslowski, J.; Stefanov, B. B.; Liu, G.; Liashenko, A.; Piskorz, P.; Komaromi, I.; Martin, R. L.; Fox, D. J.; Keith, T.; Al-Laham, M. A.; Peng, C. Y.; Nanayakkara, A.; Challacombe, M.; Gill, P. M. W.; Johnson, B.; Chen, W.; Wong, M. W.; Gonzalez, C.; Pople, J. A. *Gaussian 03*, revision C.01; Gaussian, Inc.: Pittsburgh, PA, 2003.
(23) Huber, K. P.; Herzberg, G. *Molecular Spectra and Molecular Structure: Constants of Diatomic Molecules*; Van Nostrand: New York, 1979.
(24) Luque, J.; Crosley, D. R. *J. Chem. Phys.* **1998**, *109*, 439.
(25) Kovacs, I. *Rotational Structure in the Spectra of Diatomic Molecule*; Adam Hilger Ltd.: London, 1969.
(26) Vasudev, R.; Zare, R. N.; Dixon, R. N. *J. Chem. Phys.* **1984**, *80*, 4863.
(27) Han, K. L.; He, G. Z. *J. Photochem. Photobiol., C* **2007**, *8*, 55.
(28) Alexander, M. H.; et al. *J. Chem. Phys.* **1988**, *89*, 1749.
(29) Takezaki, M.; Hirota, N.; Terazima, M. *J. Phys. Chem. A* **1997**, *101*, 3443.
(30) Lang, L. *Absorpt. Spectra Ultraviolet Visible Reg.* **1963**, *4*, 97.
(31) Sengupta, S.; Indulkar, Y.; Kumar, A.; Dhanya, S.; Naik, P. D.; Bajaj, P. N. *J. Phys. Chem. A* **2008**, *112*, 12572.

JP900567U